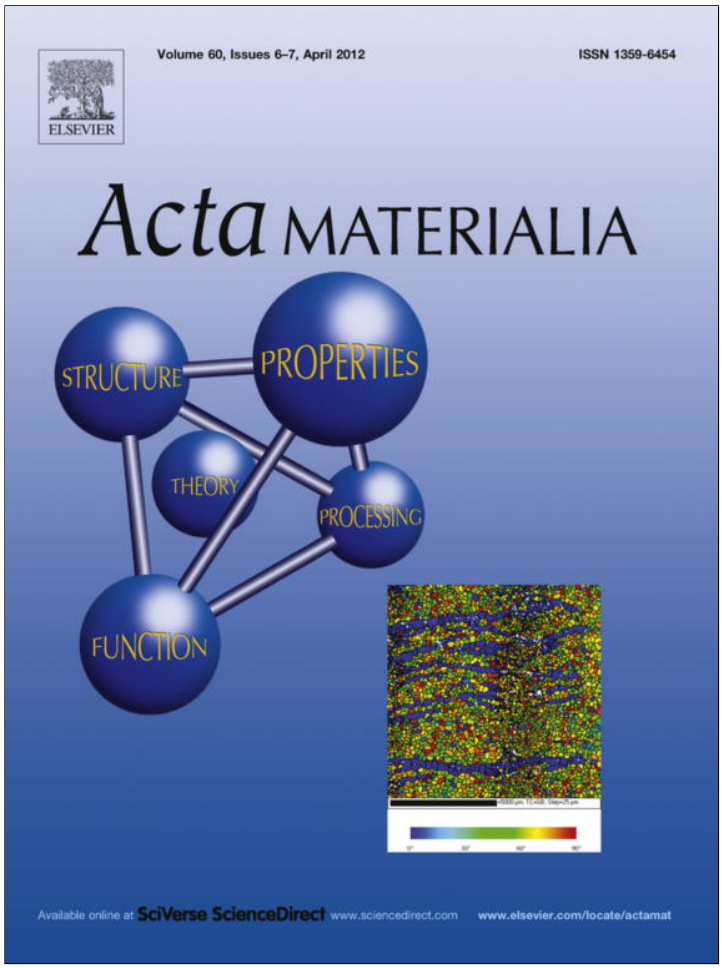

Available online at www.sciencedirect.com

SciVerse ScienceDirect

Acta Materialia 60 (2012) 2973–2981

Acta MATERIALIA

www.elsevier.com/locate/actamat

Relation between microstructure and adhesion of hot dip galvanized zinc coatings on dual phase steel

G.M. Song [a,*], T. Vystavel [b], N. van der Pers [a], J.Th.M. De Hosson [b], W.G. Sloof [a]

[a] Department of Materials Science and Engineering, Delft University of Technology, Mekelweg 2, 2628 CD Delft, The Netherlands
[b] Department of Applied Physics, Zernike Institute for Advanced Materials and Materials Innovation Institute, University of Groningen, Nijenborgh 4, 9747 AG Groningen, The Netherlands

Received 10 October 2011; received in revised form 11 January 2012; accepted 1 February 2012
Available online 6 March 2012

Abstract

The microstructure of hot dip galvanized zinc coatings on dual phase steel was investigated by electron microscopy and the coating adhesion characterized by tensile testing. The zinc coating consists of a zinc layer and columnar ζ-$FeZn_{13}$ particles on top of a thin inhibition layer adjacent to the steel substrate. The inhibition layer is a thin compact and continuous layer that consists of η-$Fe_2Al_{5-x}Zn_x$ fine and coarse particles. The coarse faceted particles are on top and fine faceted particles are at the bottom. The steel surface is covered with small fraction manganese oxides, which may impair adhesion of the zinc coating. The adhesion at various interfaces that exist in zinc-coated steel was quantitatively estimated using a so-called "macroscopic atom" model. In addition, the adhesion at the interfaces in zinc-coated steel was qualitatively assessed by examining the fracture and delamination behavior upon tensile testing. In accordance with this model, fracture along zinc grain boundaries preceded fracture along the zinc layer/inhibition layer and ζ-$FeZn_{13}$ particle/inhibition layer interfaces.

Keywords: Zinc coatings; Microstructure; Interface cracking; Work of adhesion; Coating adhesion

1. Introduction

A higher demand for safety together with the urge to reduce weight to increase fuel efficiency are driving the rapid replacement of zinc-coated low carbon steel sheets in the automotive industry with zinc-coated high strength steel sheets [1–5]. As one kind of high strength steel dual phase (DP) steels have a combination of high tensile strength, a high work hardening rate in the early stages of plastic deformation and good ductility, conferred by a complex microstructure consisting of hard martensite islands embedded in a soft ferrite matrix [4,5]. Besides these features, properties such as continuous yielding behavior, uniform plastic deformation, good formability and high dynamic energy absorption during high strain rate deformation of DP steels enable their application to improve vehicle crash performance without an increase in weight [6]. However, the alloying elements in high strength steels, such as Mn, Si, P, Al in DP steels, tend to segregate to the steel surface upon annealing at a temperature in an intercritical range between A_{C1} and A_{C3} and can be selectively oxidized prior to zinc deposition [7–12]. Thus the wettability of the surface areas covered by oxides becomes poor in a melted zinc bath, even leading to bare spot defects [11]. Consequently, adhesion of the zinc coating to the steel substrate as well as protection against corrosion is diminished [11–13]. This adhesion is crucial when zinc-coated high strength steel sheets must be deformed into the desired shape, e.g. for automotive applications [14,15].

Although various zinc coatings on steel and their deposition routes have been extensively investigated, understanding the relationship between the coating/steel interface

* Corresponding author.
E-mail addresses: g.song@tudelft.nl, songguim@yahoo.com (G.M. Song).

1359-6454/$36.00 © 2012 Acta Materialia Inc. Published by Elsevier Ltd. All rights reserved.
doi:10.1016/j.actamat.2012.02.003

chemistry and microstructure on the one hand and coating adhesion on the other remains elusive. Zinc coatings produced by hot dip galvanizing is a multi-component system consisting of several phases, such as hexagonal zinc, η-Fe_2Al_5 and ζ-$FeZn_{13}$ [14], which make analysis of the coating/substrate system difficult. Moreover, detailed knowledge about the mechanical properties of these individual phases, as well as their interfacial properties, is lacking.

Several conventional tests have been employed to evaluate the adhesion of zinc coatings to steel, such as the U-bend, V-bend, four point bend, impact, single lap shear tensile and scratch tests [14–19]. However, these methods only provide qualitative results in most cases. A quantitative evaluation is often difficult. For instance, the success of the single lap shear tensile test relies on the strength and adhesion of the glue, which must be superior to that of the zinc coatings [17,20]. To date, a reliable test method for the quantitative evaluation of the adhesive strength of zinc coatings is still lacking, but is greatly required.

A knowledge of the zinc coating adhesion, determined from the microstructure and chemical composition at the zinc coating/steel substrate interface, is crucial for the shape pressing of zinc-coated DP steel sheets for automotive industry applications [14,21]. In this study experiments have been conducted to evaluate the zinc coating adhesion of hot dip galvanized DP steel. To this end the microstructure at the interfaces of zinc-coated steel sheets was investigated by electron microscopy. Next, the work of adhesion at the interfaces was estimated using the so-called "macroscopic atom" model [22].

2. Experimental procedure

The DP steel sheet samples (220 × 120 × 1 mm), provided by Tata Group, The Netherlands, were galvanized in a RHESCA hot dip simulator. A stirrer was used to enhance movement of the liquid zinc across the steel sheet. Prior to immersion in liquid zinc at 460 °C for 3 s the steel sheet was annealed in the intercritical temperature range 705–805 °C to produce a DP microstructure (ferrite and austenite) [10]. When the steel sheet was removed from the liquid zinc bath it was immediately cooled down to room temperature in a stream of N_2 gas. The chemical composition of this steel in wt.% was 0.156 C, 1.508 Mn, 0.012 P, 0.376 Si and 0.037 Al. The molten zinc bath contained 0.19 wt.% Al.

The zinc coatings were investigated by optical microscopy (DM4000M, Leica, Germany), and the coating/steel interface microstructure was observed by scanning electron microscopy (SEM) (JSM 6500F, JEOL, Japan) equipped with for energy dispersive spectrometry (EDS) (Thermo-Fisher UltraDry detector (30 mm^2) operated with Noran System 7 software) for X-ray microanalysis. The local chemical composition was determined quantitatively using an electron probe X-ray microanalyzer (JEOL JXA 8900R WDS/EDS combined analyzer) equipped for wavelength dispersive spectrometry (WDS) operated at an electron beam energy of 5 keV to realize a spatial resolution of about 0.5 μm. The composition of the individual phases was determined by measuring the X-ray intensities of the constituent elements ($K_{\alpha 1}$ lines for Al, Si and P, $L_{\alpha 1}$ lines for Mn, Fe and Zn) after background correction relative to the corresponding intensities of reference materials (i.e. pure elements). Thus the obtained intensity ratios were processed with a matrix correction program CITZAF [23] to compute the composition with the matrix element Fe taken as the balance.

For the composition and microstructure analysis cross-sections and taper sections were prepared by successively grinding and polishing. The cross-sections were finally polished with an ion beam using a cross-section ion polisher (SM-09010, JEOL, Japan) operated at 5 keV. Taper sections were created by mounting the zinc-coated steel sample on a steel stub with an inclination angle of 5°, whereby the lateral resolution will be enhanced by a factor of about 11. After grinding and subsequent polishing the interfaces in the region between the steel substrate and the zinc coating were exposed. Samples were also prepared in which the zinc layer was removed with 5 vol.% nitric acid solution [2] to reveal the surface of the inhibition layer.

For a more detailed analysis of the composition and microstructure in the interface region transmission electron microscopy (TEM) was employed using a JEOL 2010 F-TEM operated at 200 keV. In order to prepare a cross-section of the zinc-coated steel for TEM analysis the zinc-coated steel sheet was embed in resin and then a cross-section sample was cut from this zinc-coated steel sheet. Next, this cross-section was polished and subsequently thinned to 50–100 nm by ion milling. The chemical composition analysis and phase crystalline structure identification of each phase were carried out by EDS and selected area electron diffraction (SAED). Fast Fourier transformation (FFT) of the high resolution images was performed using digital micrograph software (Gatan, Pleasanton, USA).

The residual stress in the zinc coating on the DP steel was measured by X-ray diffractometry (XRD) (Siemens D5000) using the so-called $\sin^2\psi$ method [24,25]. During the measurements the specimens were rotated around the coating surface normal with the Bragg–Brentano geometry ranging from 20° to 120° 2θ with a 0.5° step size using Cu K_a radiation [24]. The sample size was 30 × 30 × 1 mm. The Philips residual stress analysis program X'Pert was used to determine the value of the residual stresses.

The fracture and delamination behavior of the zinc-coated steel was examined using a 5 kN tensile test stage (Microtester, Deben, UK) in situ by SEM. To this end "dog-bone" samples were prepared from the zinc-coated steel sheet with a reduced section of 20 × 5 × 1 mm. After the in situ tensile deformation test cross-sections were prepared from the reduced section of the dog-bone sample. These cross-sections were also examined by SEM.

3. Work of adhesion of the interfaces present in zinc-coated steels

The work of adhesion, W_{Ad}, of an interface between phase A and phase B is the work required to separate phase A from phase B per unit interface area. It can be estimated using the "macroscopic atom" model [22,26] and is defined as:

$$W_{\mathrm{Ad}} = \gamma_A^{\mathrm{S}} + \gamma_B^{\mathrm{S}} - \gamma_{A-B}^{\mathrm{Interaction}} - \gamma_{A-B}^{\mathrm{Mismatch}} \tag{1}$$

where γ_A^{S} and γ_B^{S} are the surface energy of phase A and phase B, respectively. $\gamma_{A-B}^{\mathrm{Interaction}}$ is the interaction energy between A and B, and $\gamma_{A-B}^{\mathrm{Mismatch}}$ is the strain energy caused by the mismatch between A and B at their interface.

The "macroscopic atom" model is extended in this study to calculate the work of adhesion between different phases in a zinc-coated steel system. The surface energy of a solid solution phase containing n elements can be deduced from Song and Sloof [27] as:

$$\gamma_{A_1\ldots A_n}^{\mathrm{S}} = \sum_{i=1} nC_{A_i}^{\mathrm{S}}\gamma_{A_i}^{\mathrm{S}} - \sum_{i=1}^{n-1}\sum_{j=i+1} nC_{A_i}^{\mathrm{S}}C_{A_j}^{\mathrm{S}}\frac{\Delta H_{A_i \text{ in } A_j}^{\mathrm{Interface}}}{C_0 V_{A_i}^{2/3}} \tag{2}$$

where $C_{A_i}^{\mathrm{S}}$ is the surface fraction of element A_i in the solid solution phase A. $\Delta H_{A_i \text{ in } A_j}^{\mathrm{Interface}}$ is the interface enthalpy of one mole of element A_i in an infinitely lager reservoir of element A_j. V_{A_i} is the atom volume of A_i. C_0 is a constant that relates the atomic volume to the atomic surface area in an atomic cell, and can be taken, on average, as 4.5×10^8 [26]. For an oxide solid phase M_xO_y the surface energy can be expressed by [28]:

$$\gamma_{\mathrm{M}_x\mathrm{O}_y}^{\mathrm{S}} = \frac{C_{\mathrm{M}}^{\mathrm{S}}\Delta H_{\mathrm{M}}^{\mathrm{S}}}{\lambda^{\mathrm{M}} C_0 V_{\mathrm{M}}^{2/3}} + \frac{C_{\mathrm{O}}^{\mathrm{S}}\Delta H_{\mathrm{O}}^{\mathrm{S}}}{\lambda^{\mathrm{O}} C_0 V_{\mathrm{O}}^{2/3}} \tag{3}$$

where $\Delta H_{\mathrm{O}}^{\mathrm{S}}$ and $\Delta H_{\mathrm{M}}^{\mathrm{S}}$ are the surface enthalpies of the respective atoms O and M, and λ is the degree to which the respective surface atoms are surrounded by a vacuum. The value of λ relies on the shape of the Wigner–Seitz cell of O or M in the oxide, and might be taken, on average, as 0.31, assuming the shape of the O (or M) atomic cell as between cubic ($\lambda = 1/6$) and spherical ($\lambda = 1/2$) [26,28,29].

The interface energy between a solid phase A containing m elements (A_i, $i = 1,\ldots,m$) and a solid phase B containing n elements (B_j, $j = 1,\ldots,n$) consists of two contributions: one is related to the chemical interaction of the elements (A_i) in phase A and the elements (B_j) in phase B at the A/B interface and the other is related to the strain energy due to the mismatch between phases A and B at their interface. The contribution to the work of adhesion of the chemical interaction at the A/B interface, i.e. the interaction energy $\gamma_{\mathrm{A}_{1,\ldots,i,\ldots,m}-B_{1,\ldots,j,\ldots,n}}^{\mathrm{Interaction}}$, can be obtained from Song and Sloof [27]:

$$\gamma_{\mathrm{A}_{1,\ldots,i,\ldots,m}-B_{1,\ldots,j,\ldots,n}}^{\mathrm{Interaction}} = \sum_{i=1}^{m}\sum_{j=1} nC_{A_i}^{\mathrm{S}}C_{B_j}^{\mathrm{S}}\frac{\Delta H_{A_i \text{ in } B_j}^{\mathrm{Interface}}}{C_0 V_{A_i}^{2/3}} \tag{4}$$

where $\Delta H_{A_i \text{ in } B_j}^{\mathrm{Interface}}$ is the interface enthalpy for an element A_i fully surrounded by element B_j. If no particular orientation relationship between solid A and B is taken into account the interface can be considered as a high angle grain boundary. Hence, the mismatch energy at the interface A/B, $\gamma_{A-B}^{\mathrm{Mismatch}}$, can be estimated by [26]:

$$\gamma_{A-B}^{\mathrm{Mismatch}} = \frac{1}{3}\left(\frac{\gamma_A^{\mathrm{S}} + \gamma_B^{\mathrm{S}}}{2}\right) = \frac{1}{6}\left(\gamma_A^{\mathrm{S}} + \gamma_B^{\mathrm{S}}\right) \tag{5}$$

So when the composition of phase A (or phase B) is known, the surface energy $\gamma_{A_1\ldots A_m}^{\mathrm{S}}$ of phase A containing m elements is obtained from Eq. (2). Similarly, the surface energy $\gamma_{B_1\ldots B_n}^{\mathrm{S}}$ of the substrate B can be obtained. After that the total interaction contribution $\gamma_{\mathrm{A}_{1,\ldots,m}-B_{1,\ldots,n}}^{\mathrm{Interaction}}$ and the mismatch energy $\gamma_{A-B}^{\mathrm{Mismatch}}$ can be calculated using Eqs. (4) and (5). Finally, the work of adhesion of the interface A/B can be obtained from Eq. (1).

4. Results and discussion

4.1. Microstructure of the coating

The zinc coating is composed of zinc grains with a mean size of about 100 μm and a thickness of 10 μm (Fig. 1). High resolution images of the cross-section of the zinc-coated steel samples show columnar $FeZn_{13}$ particles (ζ-phase) on top of a thin continues inhibition layer adjacent to the steel substrate (see Fig. 2). The columnar ζ-$FeZn_{13}$ particles with a length of 1–2 μm in and diameter of 0.2–0.5 μm are on top of the inhibition layer and do not exhibit a preferential orientation. Compared with the results of Baril et al. [30], the reaction between Zn and Fe was not completely suppressed by 0.19 wt.% Al in the zinc bath in this study. It is well known that the nucleation and

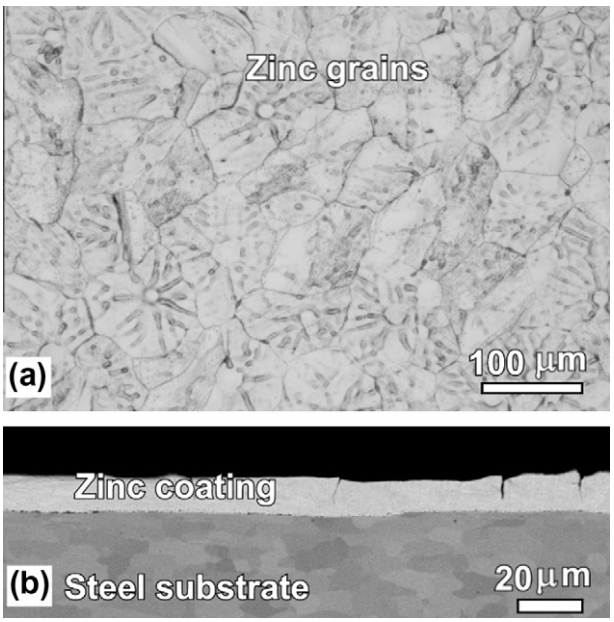

Fig. 1. (a) Optical image of the zinc coating on the dual phase steel substrate. (b) Backscatter electron image of the cross-sectional surface of the zinc-coated dual phase steel.

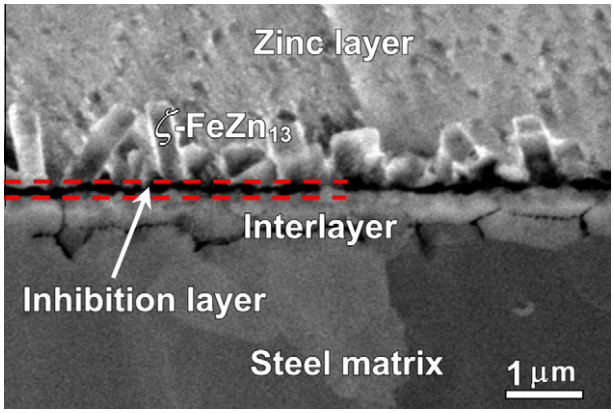

Fig. 2. SEM image of a cross-section of the zinc-coated steel, showing the zinc layer, columnar $FeZn_{13}$ (ζ) phase, continuous inhibition layer and underlayer in contact with the inhibition layer and steel matrix.

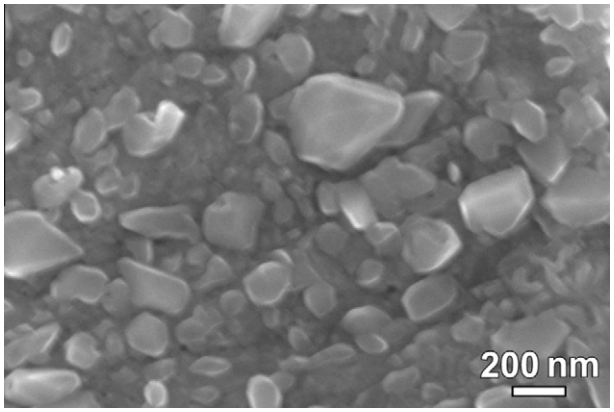

Fig. 3. SEM secondary electron image of the $Fe_2Al_{5-x}Zn_x$ inhibition layer that consists of coarse particles on top and fine particles at the bottom. The zinc layer and Fe–Zn compounds were chemically removed.

growth of Fe–Zn intermetallic compounds are not only influenced by the Al content in the zinc bath but also by other factors, such as the steel composition, zinc bath temperature, immersion time and surface roughness of the steels [30–32]. For instance, both Si and P present in the present DP steel promote the reaction of Fe with Zn to form Fe–Zn compounds (ζ-$FeZn_{13}$, δ-$FeZn_{10}$, etc.) during hot dipping, i.e. the so-called Sandelin effect [33]. Al in the zinc bath might retard the reaction of Fe with Zn via the rapid formation of η-Fe_2Al_5 compounds at the interface between the steel substrate and the melted zinc. With the formation of a continuous η-Fe_2Al_5 layer on the steel surface Fe diffusion from the steel substrate into the zinc bath will be suppressed.

Within the steel substrate a layer adjacent to the inhibition layer can be distinguished from the steel matrix (see Fig. 2). X-ray microanalysis indicates that the concentration of manganese in this layer is significantly lower than in the steel matrix; the steel matrix contains 1.8 at.% Mn while this layer contains 0.5 at.% Mn. Such a depletion of Mn within the steel subsurface of may be caused by segregation of Mn to the steel surface and ferrite grain boundaries, which was subsequently oxidized at these locations.

The inhibition layer was exposed after the zinc layer was partially delaminated from the steel substrate by deformation. The inhibition layer consists of coarse equiaxed particles with a mean size of about 200 nm on top of a compact thin layer composed of fine particles with a mean size of about 100 nm (see Fig. 3). Both the coarse and fine particles are composed of η-$Fe_2Al_{5-x}Zn_x$ phase containing a small fraction of zinc (3.5–7.5 at.%), as identified by TEM and X-ray microanalysis.Al reacts rapidly with the steel surface to form a Fe–Al compound when a steel sheet is dipped into a molten zinc bath containing some Al. Then the η-$Fe_2Al_{5-x}Zn_x$ phase nucleates at the steel surface and grows into the liquid zinc. A rapid reaction between Al and Fe occurs if sufficient Al is supplied via liquid-state diffusion of Al from the molten zinc to the inhibition layer. However, if the supply of Al is insufficient (e.g. when the Al content in the zinc bath is lower than 0.10 wt.% [32]) the inhibition layer will be thin and, consequently, more Fe will diffuse into the liquid zinc to form Fe–Zn compounds. These compounds, usually ζ-$FeZn_{13}$, nucleate on top of the inhibition layer. Hence, Fe diffuses from the steel substrate into the zinc bath through the solid inhibition layer. If only bulk diffusion is taken into account the diffusion coefficient of Fe atoms through the inhibition layer can be roughly estimated as $D = D_0 \exp(-Q/RT)$, where D_0 is the pre-exponential factor (3.48×10^{-7} m^2 s^{-1}), Q is the activation energy for diffusion (139 J mol^{-1}), R is the gas constant (8.31 J mol^{-1} K^{-1}) and T (K) is the temperature of the steel [34]. Thus the diffusion coefficient at 460 °C is 4.30×10^{-17} m^2 s^{-1}. The solid inhibition layer suppresses the dissolution of Fe in the melted zinc bath [34] and, in turn, the subsequent nucleation and growth of Fe–Zn compounds, such as ζ-$FeZn_{13}$, at the steel surface are retarded. When the Al concentration in the zinc bath is higher than 0.15 wt.% the inhibition layer might effectively suppress the formation and growth of Fe–Zn compounds [32]. The present observations (Fig. 2) on zinc coatings suggest that growth of the Fe–Zn compound layer (like ζ-$FeZn_{13}$ layer) was suppressed at about 1 μm thickness. Thus the relatively high Al content (0.19 wt.%) in the zinc bath in this study is beneficial in the development of an effective inhibition layer.

4.2. Chemical composition analysis

Maps of the distribution of Mn, Al and O near the zinc coating/steel interface as recorded by X-ray microanalysis in TEM are shown in Fig. 4. A continuous thin layer with a high Al concentration representing the $Fe_2Al_{5-x}Zn_x$ inhibition layer was observed. A locally high Mn concentration associated with a high oxygen concentration was detected. This phase is identified as amorphous manganese oxides (see Fig. 5). This manganese oxide phase is mainly located at the interface between the steel matrix and the inhibition layer (Fig. 5a), and also occasionally at ferrite grain

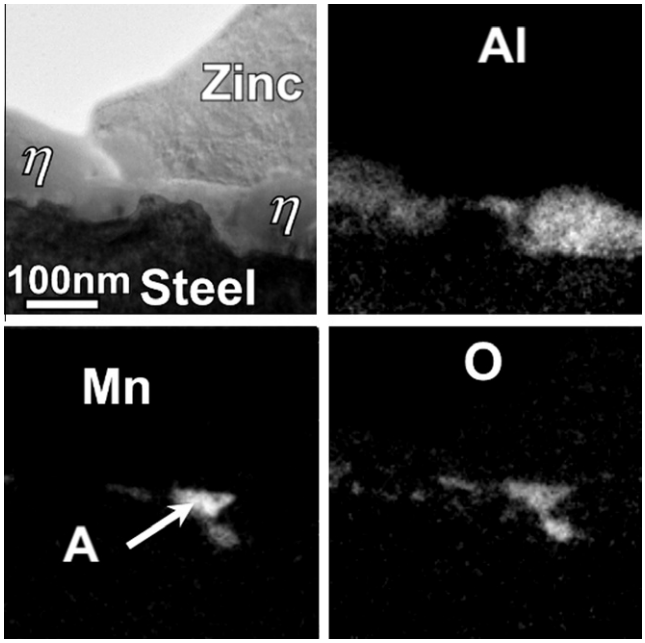

Fig. 4. Element distribution of Al, Mn and O near the zinc coating/steel interface as observed on a cross-section of the zinc-coated steel by TEM using energy dispersive X-ray spectrometry. η represents the $Fe_2Al_{5-x}Zn_x$ phase. The presence of manganese oxide at the steel surface is evident.

boundaries in the adjacent layer (Fig. 5b). Mn in the steel substrate has a low equilibrium oxygen potential (Mn $10^{-29.6}$ atm, 1 atm = 1.01×10^5 Pa) [8], so it is expected to be oxidized at the steel surface or at some ferrite grain boundaries when the steel is exposed to air and oxygen diffuses into the steel along ferrite grain boundaries (fast diffusion paths) [35], which results in enrichment of Mn at the steel surface or at grain boundaries during the annealing process.

4.3. Fracture behavior of zinc coating

In situ SEM observation of the cracking behavior of the zinc coating under tensile loading shows that cracks mainly occurred along the zinc grain boundaries (Fig. 6a) These cracks were arrested at the coating/steel interface, and then propagated along the coating/steel interface, rather than penetrating into the steel substrate, which resulted in a segmented fractured coating (Fig. 6b). An investigation by Aden-Ali et al. [36] on zinc-coated steel also shows that the cracks arising in the zinc coating were confined to the coating and stopped at the zinc–steel interface, with debonding at higher stresses, which is consistent with our present observations. The grain boundaries in the zinc coating are weak sites due to the presence of voids and pre-existing microcracks after hot dipping (see Fig. 6c). The voids may be caused by significant shrinkage (about 8.3 vol.%) upon solidification of the zinc [37]. The microcracks may be induced by the large thermal misfit stress between the solid zinc coating and the steel substrate after cooling from the solidification temperature (at about 419 °C) to room temperature. The average thermal expansion coefficient of

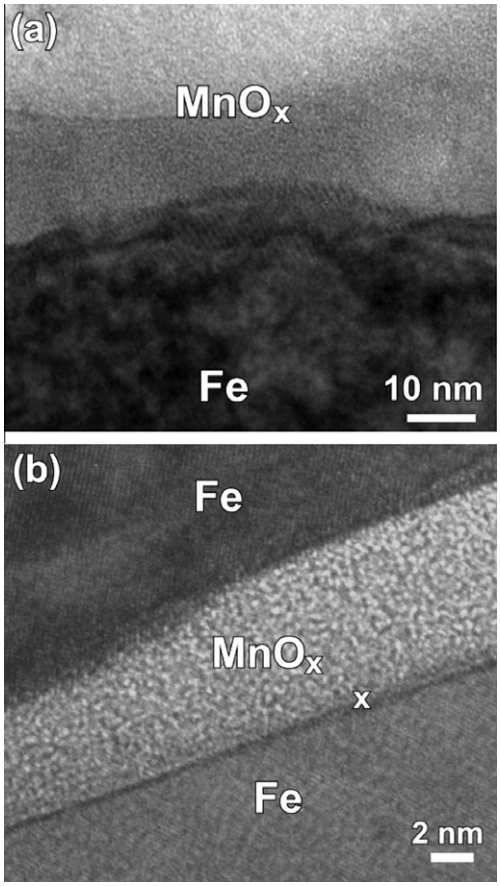

Fig. 5. High resolution TEM image of the amorphous manganese oxide present at (a) the zinc coating/steel interface and (b) the ferrite grain boundary within the steel substrate just beneath the zinc coating/steel interface.

the zinc is 3.02×10^{-5} per K, whereas the thermal expansion coefficient of the steel substrate is 1.18×10^{-5} per K [37]. If the difference in thermal shrinkage upon cooling is fully accommodated elastically by the zinc coating, considering that the elastic modulus and Poisson ratio for zinc are 70 GPa and 0.3 [38], respectively, then the misfit stress in the zinc coating will be about 725 MPa at room temperature. However, the residual stress as determined by XRD is much lower, about 100 MPa. Thus a major part of the thermal misfit has been accommodated by plastic deformation of the zinc grains and the formation of microcracks along the zinc grain boundaries.

Large stresses develop at the edges of the segmented zinc coating along the interface of the coating with the substrate [20], which causes subsequent cracking along the coating/steel interface (see Fig. 7a). Detailed analysis of cross-sections of the delaminated coating/steel interface revealed that the cracks propagated mainly along the zinc layer/inhibition layer and ζ-$FeZn_{13}$ particle/inhibition layer interfaces, rather than the inhibition layer/steel interface, which demonstrates that both the adhesion of the zinc layer/inhibition layer and ζ-$FeZn_{13}$ particle/inhibition layer interfaces are lower than the adhesion of the inhibition layer/steel interface. This is confirmed by an examination

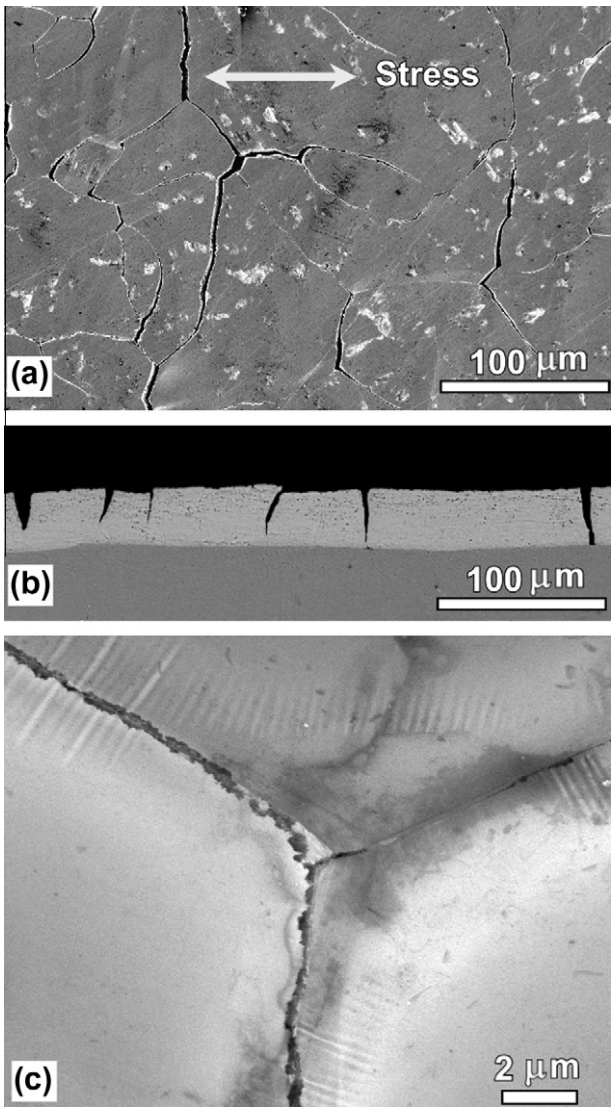

Fig. 6. SEM secondary electron images of the zinc coating surface. (a) Fracture along zinc grain boundaries after 4% tensile strain. (b) The segmented zinc coating after 4% tensile strain. (c) The presence of microvoids and microcracks along zinc grain boundaries before tensile deformation.

of the fracture surface after zinc coating delamination. The steel substrate after coating delamination is mainly covered with η-$Fe_2Al_{5-x}Zn_x$ particles of the inhibition layer (spot A in Fig. 7b). η-$Fe_2Al_{5-x}Zn_x$ particles are absent from only a few spots at this fracture surface. At these locations high concentrations of Mn and O were detected (spot B in Fig. 7b). Apparently, delamination also occurred along the interface between Mn oxides and the inhibition layer, which is thus a weaker interface. Some remnants of the columnar ζ-$FeZn_{13}$ particles on the fracture surface after coating delamination were observed (see Fig. 8a). It seems that these particles were pulled out of the zinc matrix upon delamination, suggesting that the ζ-$FeZn_{13}$ particle/η-zinc matrix interface is weak. Complete delamination of the zinc coating from the steel substrate was not observed even after the zinc-coated steel fractured at an applied tensile strain of

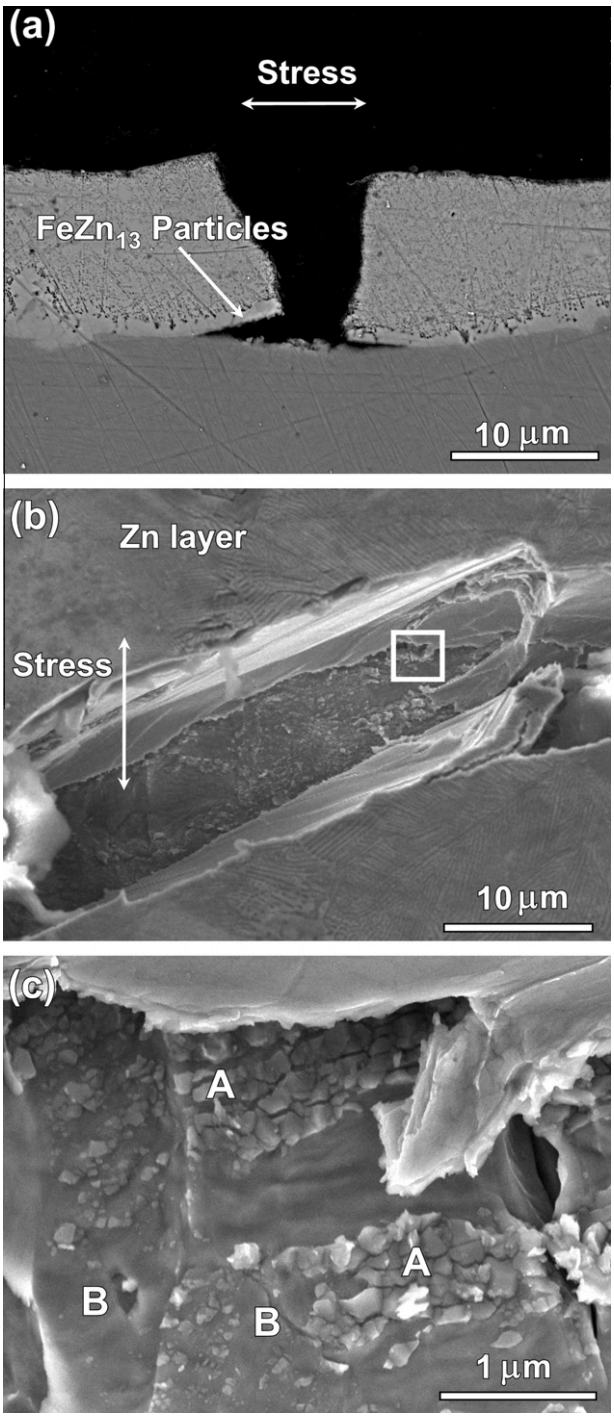

Fig. 7. SEM secondary electron images of partial zinc coating delamination after 13% tensile strain. (a) Cross-section. (b) Top view of the cracked coating. (c) An enlarged image of the location remarked with a white box in (b). The $Fe_2Al_{5-x}Zn_x$ inhibition layer (point A) and some areas covered with Mn oxides (point B) are seen in (c).

about 30%. In order to investigate the adhesive properties of the ζ-$FeZn_{13}$ particle/η-zinc matrix interface the zinc coating was locally thinned to about 1 μm thickness by mechanical polishing and then subjected to tensile deformation. Note that the average length of columnar ζ-$FeZn_{13}$ is about 1 μm. The microcracks initiated at the ζ-$FeZn_{13}$/Zn

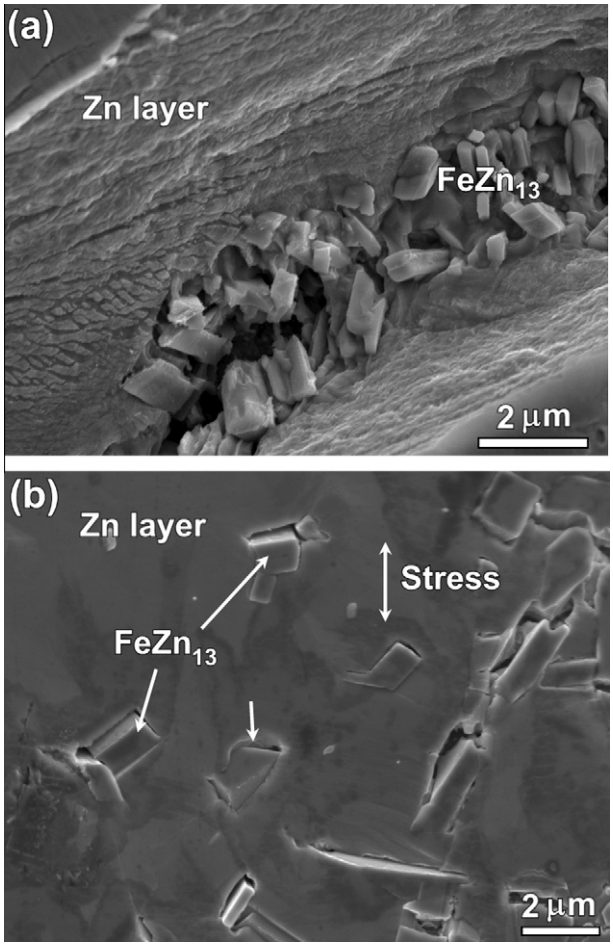

Fig. 8. Cracked zinc coating. (a) Remnants of $FeZn_{13}$ particles at the fracture surface of the zinc layer. (b) Microcracks initiated at the $FeZn_{13}$ particle/Zn matrix interface (here the zinc coating surface was thinned by polishing).

interface, preceded coating delamination, as shown in Fig. 8b. This experimental evidence suggests that the ζ-$FeZn_{13}$/η-Zn interface is weaker than the zinc layer/inhibition layer interface.

4.4. Work of adhesion of interfaces

The chemical compositions of the zinc layer, ζ-$FeZn_{13}$ particle, inhibition layer (η-$Fe_2Al_{5-x}Zn_x$) and steel substrate measured by EPMA are presented in Table 1. The surface energy of each element and the interface enthalpy of each element fully surrounding by another element as tabulated in Boer et al. [26] are used for the present calculations. The surface energies of these phases and the work of adhesion of the corresponding interfaces between the above components are calculated using the measured chemical compositions (see Tables 2 and 3). In order to estimate the influence of the Mn oxide (assumed to be MnO) existing at the zinc coating/steel interface on coating adhesion the work of adhesion of the oxide/steel and zinc coating/oxide interfaces are also calculated.

The work of adhesion of the ζ-$FeZn_{13}$/η-Zn interface is 1.66 J m^{-2}, the lowest among all of the interfaces listed in Table 3, which implies that adhesion of the ζ-$FeZn_{13}$/η-Zn interface might be the weakest. SEM observations of the cracking behavior of the ζ-$FeZn_{13}$/Zn interface is consistent with this calculated work of adhesion (see Fig. 8b). The work of adhesion of the η-Zn/η-$Fe_2Al_{5-x}Zn_x$ and ζ-$FeZn_{13}$/η-$Fe_2Al_{5-x}Zn_x$ interfaces are 2.03 and 2.12 J m^{-2}, respectively, which are close to that of the ζ-$FeZn_{13}$/η-Zn interface (1.66 J m^{-2}). The η-$Fe_2Al_{5-x}Zn_x$/steel interface with a work of adhesion of 3.54 J m^{-2} is expected to be the strongest.

Although the ζ-$FeZn_{13}$/η-Zn interface is the weakest, and thus may govern the delamination behavior of the zinc coating, the columnar ζ-$FeZn_{13}$ particles are embedded in the zinc matrix and do not form a continuous compact layer. Thus cracks initiated at the weakest $FeZn_{13}$/η-Zn interface are easily arrested by plastic deformation of the zinc matrix. As an alternative route, cracks might occur at the weaker η-Zn/η-$Fe_2Al_{5-x}Zn_x$ and ζ-$FeZn_{13}$/η-$Fe_2Al_{5-x}Zn_x$ interfaces and then propagate along these interfaces, resulting in coating delamination. The predicted cracking behavior is in good agreement with the experimental observations (see Fig. 6a). Adhesion of the zinc coating to steel can be enhanced if the formation of ζ-$FeZn_{13}$ particles is suppressed. This may be achieved by increasing the Al content in the zinc bath to 0.15 [32] or 0.20 wt.% [39] and reducing the immersion time (to a few seconds) to suppress the nucleation and growth of ζ-$FeZn_{13}$ particles.

The work of adhesion of the η-Zn/MnO and η-$Fe_2Al_{5-x}Zn_x$/MnO interfaces are 2.17 and 3.34 J m^{-2}, respectively, and both are lower than that of the η-$Fe_2Al_{5-x}Zn_x$/steel interface (3.54 J m^{-2}). Thus the presence of oxide at the steel surface weakens coating adhesion to the steel substrate by inserting weaker η-Zn/oxide and η-$Fe_2Al_{5-x}Zn_x$/oxide interfaces between the zinc layer (or inhibition layer) and steel substrate. Moreover, thermal

Table 1
Chemical composition of the phases present in zinc-coated dual phase steel (at.%).

Phase	Fe	Zn	Al	Mn	Si
Zinc layer (η-Zn)	0.1	99.8	0.1	0	0
Steel substrate (Fe)	97.4	0	0	1.8	0.8
Inhibition layer (η-$Fe_2Al_{5-x}Zn_x$)	26.2	6.5	67.3	0	0
ζ-$FeZn_{13}$	7.5	92.4	0.1	0	0

Table 2
Surface energies of various phases at 298 K (J m^{-2}).

Phase	Surface energy
Zinc layer (η-Zn)	0.94
Steel substrate (Fe)	2.39
Inhibition layer (η-$Fe_2Al_{5-x}Zn_x$)	1.48
ζ-$FeZn_{13}$	1.04
MnO	1.55

Table 3
Predicted energies of various interfaces at 298 K (J m^{-2}).

	Interaction energy	Mismatch energy	Work of adhesion
η-Zn/η-$Fe_2Al_{5-x}Zn_x$	−0.01	0.40	2.03
ζ-$FeZn_{13}$/η-Zn	−0.01	0.33	1.66
ζ-$FeZn_{13}$/η-$Fe_2Al_{5-x}Zn_x$	−0.02	0.42	2.12
η-$Fe_2Al_{5-x}Zn_x$/steel	−0.32	0.65	3.54
η-$Fe_2Al_{5-x}Zn_x$/MnO	−0.27	0.51	2.79
η-Zn/MnO	−0.10	0.42	2.17
Steel/MnO	−0.06	0.66	3.34

residual stresses would be introduced in the zinc coating/steel interface region due to differences in the expansion coefficients of the oxide, inhibition layer and steel substrate. Our experimental observations indicate that cracks occurred along the interface between the zinc layer (or inhibition layer) and the oxide (see Fig. 7c), which correlates well with the prediction for the work of adhesion. On the other hand, the presence of oxides at the steel surface severely decreases its wettability in the molten zinc bath during hot dipping process, and consequently results in bare spots (i.e. steel surface not covered by zinc) [40–42]. Additionally, oxidation at the steel surface also decreases the mechanical properties of steels [43]. Thus any oxide at the steel surface should be completely removed prior to zinc coating deposition in order to achieve sound coating adhesion.

The experimental results in the present work, which are in agreement with the predictions for the work of adhesion, have shown that adhesion of the zinc coating can be enhanced by suppressing the formation of Fe–Zn compounds and oxides at the interface between the zinc coating and the steel substrate.

5. Conclusion

The zinc coating on DP steels consists of a zinc layer and columnar ζ-$FeZn_{13}$ particles on top of a thin inhibition layer next to the steel substrate. The inhibition layer contains faceted η-$Fe_2Al_{5-x}Zn_x$ particles on top of a thin compact continuous layer, which is composed of lenticular η-$Fe_2Al_{5-x}Zn_x$ particles. Segregation and oxidation of manganese at the steel surface occurred before zinc coating deposition on the steel.

Cracking along zinc grain boundaries is preceded by fracture along the zinc layer/inhibition layer and ζ-$FeZn_{13}$ particle/inhibition layer interfaces. When Mn oxide is present at the interface with the zinc coating or inhibition layer fracture also occurs along these interfaces. In agreement with predictions for the work of adhesion of the various interfaces in the zinc coating/steel substrate region zinc coating delamination preferentially occurs along the zinc layer/inhibition layer and ζ-$FeZn_{13}$ particle/inhibition layer interfaces, rather than the inhibition layer/steel interface.

The adhesion of a zinc coating to DP steels can be improved by avoiding the formation of Fe–Zn compounds and oxides at the interface between the zinc coating and the steel substrate. A sufficient amount of Al in the zinc bath and a reduction in oxide formation during annealing, prior to the zinc coating deposition, are beneficial.

Acknowledgements

This research was carried out under Project No. MC7.00075A within the framework of the strategic research program of the Materials Innovation Institute (M2i, www.m2i.nl), the former of the Netherlands Institute for Metals Research. The authors are indebted to Ir Bart van Veldhuizen and Dr Margo Vlot of Tata Steel (formerly CORUS), IJmuiden, The Netherlands, for stimulating discussions.

References

[1] Chen L, Fourmentin R, McDermid JR. Metall Mater Trans 2008;39:2128.
[2] Karduck P, Wirth T, Pries H, Fresenius J. Anal Chem 1997;358:135.
[3] Wichern CM, De Cooman BC, Van Tyne CJ. Acta Mater 2004;52:1211.
[4] Jordan CE, Goggins KM, Marder AR. Metall Mater Trans A 1994;25A:2101.
[5] Petit EJ, Grosbety Y, Aden-Ali S, Gilgert J, Azari Z. Surf Coat Technol 2010;205:2404.
[6] Belhouse EM, Mertens AIM, McDermid JR. Mater Sci Eng A 2008;463:147.
[7] Khondker R, Mertens AIM, McDermind JR. Mater Sci Eng A 2008;463:157.
[8] Maki J, Mahieu J, De Cooman BC, Claessens S. Mater Sci Technol 2003;19:125.
[9] Mariaux A, Rappaz M. Acta Mater 2011;59:927.
[10] Wu H, Hol CWJ, Van Popta PJ, Verloop WCH. Patent WO2008/104610 A1; 2008.
[11] Mintz B. Inter Mater Rev 2001;46:174.
[12] Hertveldt I, De Cooman BC, Claessens S. Metall Mater Trans A 2000;31A:1225.
[13] Song GM, Sloof WG, Vystavel T, De Hosson JTM. Mater Sci Forum 2007;539–543:1104.
[14] Marder AR. Prog Mater Sci 2000;45:191.
[15] Tzimas E, Papadimitriou G. Surf Coat Technol 2001;145:176.
[16] De Bruycker E, De Cooman BC, De Meyer M. Steel Res Int 2004;75:147.
[17] Ye M, Delplancke JL, Berton G, Segers L, Winand R. Surf Coat Technol 1998;105:184.
[18] Hertveldt I, De Cooman BC, Meseure K, Xhoffer C. ISIJ Int 1999;39:1280.
[19] Gallego A, Gil JF, Vico JM, Ruzzante JE, Piotrokowski R. Scripta Mater 2005;52:1069.
[20] Song GM, Sloof WG, Pei YT, De Hosson JTM. Surf Coat Technol 2006;201:4311.
[21] Nakai K, Okamoto T, Ohtsubo H. ISIJ Int 2004;44:914.
[22] Miedema AR. J Less-Common Met 1973;32:117.
[23] Armstrong JT. Microbeam Anal 1995;4:177.
[24] Clemens BM, Bain JA. MRS Bull 1992;17:46.
[25] Sloof WG, Kooi BJ, Delhez R, De Keijser TH, Mittemeijer EJ. J Mater Res 1996;11:1440.
[26] Boer FR, Boom R, Mattens WCM, Miedema AR, Niessen AK. Cohesion in metals: transition metals alloys. Amsterdam: North-Holland Physical Publishing; 1989.

[27] Song GM, Sloof WG. Surf Coat Technol 2011;205:4632.
[28] Bennett IJ, Kranenburg JM, Sloof WG. J Am Ceram Soc 2005;88:2209.
[29] Jeugens LPH, Sloof WG, Tichelaar FD, Mittemeijer EJ. Phys Rev B 2000;62:4707.
[30] Baril E, L'Esperance G. Metall Mater Trans A 1999;30A:681.
[31] Culcasi JD, Sere PR, Elsner CI, Di Sarli AR. Surf Coat Technol 1999;122:21.
[32] Nakamori T, Adachi Y, Toki T, Shibuya A. ISIJ Int 1996;36:179.
[33] Mishra R, Dutta M. ISIJ Int 2007;47:1504.
[34] O'Dell S, Charles J, Vlot M, Randle V. Mater Sci Technol 2004;20:251.
[35] Feliu S, Pérez-Revenga ML. Metall Mater Trans A 2004;35A:2039.
[36] Aden-Ali S, Chamat A, Gilgert J, Petit EJ, Dominiak S, Schmitt L, et al. Eng Fail Anal 2009;16:2009.
[37] Lide DR. Handbook of chemistry and physics. 76th edn. Boca Raton, FL: CRC Press; 1995.
[38] Morga SWK. Zinc and its alloys. London, UK: Macdonald & Evans Ltd; 1977. p. 7.
[39] Jordam CE, Zuhr R, Marder AR. Metall Mater Trans A 1997;28A:2695.
[40] Vanden EX, Servais JP, Lamberigts M. In: Proceeding of Galvatech '04. Warrendale, PA: Association for Iron and Steel Technology; 2004. p. 361.
[41] Drillet P, Zermout Z, Bouleau D, Mataigne J, Claessens S. In: Proceeding of Galvatech '04. Warrendale. PA: Association for Iron and Steel Technology; 2004. p. 1123.
[42] Alibeigi S, Kavitha R, Meguerian RJ, McDermid JR. Acta Mater 2011;59:3537.
[43] Azari A, Abbadi M, Moustabchir H, Lebienvenu M. Int J Fatigue 2008;30:517.